https://doi.org/10.5194/egusphere-2025-48
Preprint. Discussion started: 24 January 2025

Anvil-radiation diurnal interaction: Shortwave radiative-heating destabilization driving the diurnal variation of convective anvil outflow and its modulation on the radiative cancellation

Zhenquan Wang[1, *]

[1] School of Atmospheric Sciences, Nanjing University, Nanjing, China

Correspondence to: Zhenquan Wang (zhqwang@smail.nju.edu.cn)

Abstract. The behavior of convection producing the anvil is neither well derived from current available observations nor well represented in models. In this work, a novel convective cloud data product is designed to capture the convective anvil outflow. Convective organizations and life stages are derived from the images of infrared brightness temperature (BT) of geostationary (GEO) satellites based on a variable-BT segment tracking algorithm, which brings the possibility for quantifying the convective anvil outflow. Vertical structures of convection are measured by sensors of the A-Train Constellation, which provides the cross section of convective outflow. Here, GEO-based convective tracking and A-Train-detected cloud vertical profiles are combined to develop a novel comprehensive GEO-A-Train merged (GATM) convective cloud data product for investigating the process of convective anvil outflow.

On the basis of this novel Lagrangian-view GATM data, the anvil production for mesoscale convective systems (MCSs) can be quantified. The results show that daytime MCSs can produce more anvil clouds than nighttime MCSs. During the daytime, shortwave radiative heating destabilizes the MCS top and invigorates the top-heavy circulation to promote the anvil outflow, whereas during the nighttime longwave radiative cooling stabilizes the MCS top and weakens the circulation to hinder the anvil outflow. Moreover, approximately 11 W m^{-2} for cloud radiative effects are modulated by the diurnal variation of convective outflow. Overall, this work presents the observed anvil-radiation diurnal interaction process: radiative heating determines the diurnal variation of anvil outflow; in turn, the diurnal variation of anvil outflow determines the Earth radiative budget.

1. Introduction

Anvil clouds have strong interactions with radiation. Tropical convective regions are usually characterized by abundant convective activities and anvil clouds (Yuan and Houze, 2010). Nevertheless, the longwave (LW) and shortwave (SW) cloud radiative effects (CREs) of tropical anvil clouds are both large to cancel each other, namely radiative near cancellation (Kiehl, 1994). The final net radiation of tropical convective regions is nearly the same as that of non-convective regions (Hartmann and Berry, 2017). If the radiative cancellation is disturbed, the radiative impacts of anvil clouds on the Earth would be easily amplified to form strong feedback process with the climate, which is the leading uncertainty in the climate sensitivity simulated by climate models (Bretherton, 2015; Hartmann, 2016; Sherwood et al., 2020). The possibility of some not yet understood feedback processes that result in the radiative near cancellation cannot be ruled out (Hartmann, 2016).

The radiative near cancellation is by no means guaranteed in the future climate change (Gettelman and Sherwood, 2016). The determinant of the radiative cancellation is important for modulating the Earth radiative budget, and is the bridge of the anvil interacting with the climate. Two theories have been proposed for explaining the radiative near cancellation, but no definite full answer has been provided until now (Hartmann, 2016). Kiehl (1994) argued that the major determinant of the near cancellation is the cloud-top height that has a weak dependence on the sea surface temperature (SST), and thus the near

https://doi.org/10.5194/egusphere-2025-48
Preprint. Discussion started: 24 January 2025

cancellation across warm and cold oceans is a fortuitous coincidence. As the climate warms, the cloud-top height will rise to enhance the cancellation between LW and SW CREs, which allows the anvil to trap more outgoing LW radiation to form a positive feedback process with the climate (Zelinka and Hartmann, 2010). In addition, Hartmann and Berry (2017) argued that the radiative near cancellation is caused by the offset between the negative CREs of rainy cores and the positive CREs of the non-precipitating anvil clouds. Since the anvil production of convection depends strongly on radiative heating profiles, the radiative near cancellation is constrained by the cloud radiative heating. On the basis of this hypothesis, the reduction of anvil areas can weaken the radiative cancellation to impose negative feedback on the climate (or vice versa).

These two hypotheses provide basic physical understandings for the anvil altitude and coverage climate feedback mechanisms, respectively. However, there is still a lack of consideration of the radiative cancellation caused by the diurnal variation of convective anvil outflow. At daytime, only optically thin cirrus clouds have net warming CREs. However, no matter what the thickness is, nocturnal clouds always have net warming effects on the Earth. These nocturnal clouds can help to compensate the daytime net cooling effects to promote the radiative cancellation. As a result, the diurnal variation of convective anvil outflow determines the degree of radiative cancellation fundamentally.

Although the theory of the radiative cancellation modulated by the diurnal variation of convective anvil outflow is rather simple, the diurnal variation of convective anvil outflow has not been well investigated before. Owing to insufficient sub-grid-scale and microphysical processes in climate models, the parameterized process of convective outflow is dependent on the parameter setting and not deemed trustworthy (Clement and Soden, 2005; Suzuki et al., 2013; Zhao, 2014; Sherwood et al., 2020), and the diurnal cycle of clouds in climate models has significant biases (Yin and Porporato, 2017; Chen et al., 2022; Zhao et al., 2023). Due to the uncertainty in the sub-grid turbulence and microphysical processes of cloud-resolving models, the convective anvil outflow still cannot be well simulated (Matsui et al., 2009; Powell et al., 2012; Zeng et al., 2013; Bretherton, 2015; Atlas et al., 2024). In observations, the organized convective structures and the links between convection and anvil clouds are poorly resolved and the convective life-cycle information is not provided in the widely-used Euler-view grid data set, such as the International Satellite Cloud Climatology Project (ISCCP) cloud data product (Rossow and Schiffer, 1991) and the Clouds and the Earth's Radiant Energy System (CERES) project (Minnis et al., 2011; Doelling et al., 2016). In a Lagrangian view, many convections of different life stages are usually clustered and their outflowing anvil clouds are merged in complex convective organizations (CCOs) (Yuan and Houze, 2010; Yuan et al., 2011; Wang and Yuan, 2024). Traditional tracking algorithms poorly distinguish the process of convective anvil outflow, since those anvil clouds that are contributed by many different convections are mixed in traditional fixed-threshold tracking (Wang and Yuan, 2024).

On the basis of hourly infrared brightness temperature (BT) images of geostationary satellites (GEOs), a novel adaptive variable-BT segment tracking algorithm has been proposed to partition the CCO into single-cold-core structures for tracking separately (Wang and Yuan, 2024). Non-precipitating anvil clouds are explicitly associated with unique cold cores. As a result, an advantage of this novel tracking algorithm is to quantify the anvil outflow for the duration of convection in CCOs. GEO observations and the novel variable-BT segment tracking algorithm provide a foundation to capture the convective anvil outflow. Nevertheless, due to the limitation of passive sensors, the convective vertical structures are not well detected by the GEO radiometer imager. Active sensors of A-Train Constellation, such as Cloud-Aerosol Lidar and Infrared Pathfinder Satellite Observations (CALIPSO) Cloud-Aerosol Lidar with Orthogonal Polarization (CALIOP) and CloudSat Cloud Profiling Radar (CPR), can detect the cloud vertical structures (Stephens et al., 2002). But, the A-Train satellite orbit is sun-synchronous and only observations around 1:30 and 13:30 local time (LT) are available, which are too sparse to track storms or to provide a full picture of convective organizations. It seems that the advantages of GEO and A-Train satellite observations are complementary for describing convective outflow processes in 4 dimensions of space and time.

In this work, on the basis of the novel variable-BT segment tracking algorithm, the GEO-based convective tracking and cloud vertical profiles from A-Train satellites are combined to develop a novel comprehensive 4-D GEO-A-Train merged

https://doi.org/10.5194/egusphere-2025-48
Preprint. Discussion started: 24 January 2025

(GATM) convective cloud data product for convective anvil outflow. With this novel 4-D GATM convective cloud data product, the anvil-radiation interaction is systematically investigated on the diurnal time scale for two interactive processes:

(1) How does the radiation influence diurnal variation of convective anvil outflow?

(2) How does the diurnal variation of convective anvil outflow influence the radiative cancellation?

This work is laid out as follows: Section 2 introduces the data and methods; Section 3 shows the diurnal variation of convective anvil outflow and its modulation by radiative heating, to answer the first question; Section 4 evaluates the sensitivity of the radiative cancellation to the diurnal variation of convective outflow, to answer the second question. Section 5 presents conclusions.

2. Data and methods

Section 2 introduces data and methods. Section 2.1 introduces the convective tracking algorithm and data set, which were developed in Wang and Yuan (2024). Section 2.2 introduces a novel 4-D GATM convective cloud data product by combining GEO-based convective tracking and A-Train satellite-detected cloud vertical profiles, which is developed in this work. Section 2.3 introduces the study domain that this work focuses on. Section 2.4 introduces statistical methods used in this work.

2.1 GEO-based adaptive variable-BT segment tracking data set

Tropical convection usually has complicated organizations and behaviors. It has long been observed that most of mesoscale convective systems (MCSs) are not isolated convective bodies but many MCSs are connected and clustered in a large CCO (Yuan and Houze, 2010; Yuan et al., 2011; Yuan and Houze, 2013). Those MCSs that are connected in CCOs could be initiated at different times and be in different life stages, but their produced anvil clouds are mixed in CCOs. On the basis of hourly GEO BT images at 10.8 μm, Wang and Yuan (2024) have developed a novel variable-BT segment tracking algorithm to partition the CCO into organization segments (OSs) of single cold cores and then to track OSs separately. Here, these OSs can also be understood as convective activities with core structures in CCOs. This algorithm can track the structural evolution of OSs and the anvil production for their durations.

On the basis of hourly GEO images, the steps of the variable-BT segment tracking algorithm are briefly introduced as follows:

(1) **Identification and segmentation of OSs in CCOs:** A set of adaptively variable BT thresholds from 180-260 K per 5-K interval and a minimum area threshold of 1000 km^2 are used to identify the CCO structures, i.e., cold cores (the local coldest BT isotherm), cold centers (the warmest BT isotherm of enclosing only one cold core). These identified core structures are used to distinguish different convective activities clustered in CCOs. For their segmentation, the pixels lying outside the centers are assigned to the centers iteratively by the 1-K interval on the basis of the nearest route distance (Figure 2 in Wang and Yuan (2024)), which requires that the outflowing anvil clouds must be connected with its origin of cold cores. In this way, anvil clouds in CCOs are explicitly associated with unique cold cores. And the OS is a well-organized single-core structure in 3 dimensions (x, y and BT), in which the cold-core BT can represent its developing strength.

(2) **Tracking OSs via dynamic overlaps:** Dynamic overlaps combine the cross correlation and area overlaps for tracking, and refer to the overlap in areas after moving OSs to the position predicted by cross correlation. For two OSs with sufficient dynamic overlap in their major core structures exceeding 50%, they are deemed the same convection at different times. The life cycle of a convective activity clustered in CCOs refers to these temporally associated OSs. The convective peaking strength is measured by the cold-core-peak BT, which is defined as the coldest cold-core BT in life cycles. The life

https://doi.org/10.5194/egusphere-2025-48
Preprint. Discussion started: 24 January 2025

cycle is separated into two stages of the development and decay, which are discriminated by the cold-core peaking time of the coldest BT with the largest core area.

In this tracking dataset, the spatial resolution is 0.05° and the temporal resolution is 1 hour. For precipitation, the hourly fine-scale global precipitation measurement (GPM) is collocated with the GEO BT images to provide estimates of pixel-level precipitation (Huffman, 2023). For the all-sky radiative flux at the top of the atmosphere (TOA), the hourly broadband shortwave albedo (β) and outgoing longwave radiation (OLR) images of 0.05° are derived from the GEO radiometers. The hourly TOA insolation and the broadband clear-sky upwelling longwave outgoing and shortwave reflected radiative flux at each grid of 0.05° are allocated from the Clouds and the Earth's Radiant Energy System (CERES) synoptic 1-degree (SYN1deg) product (Doelling et al., 2016). The CREs are defined as the difference of the predicted TOA clear-sky upwelling radiative flux relative to the observed TOA all-sky radiative flux.

Yuan and Houze (2010) have defined the MCSs as the segmented single-core OSs of heavy precipitations (6 mm/hour) and cold-core BT colder than 220 K. Similarly, the MCSs in this work refer to the OS of the heavy precipitation (6 mm/hour) areas larger than 1000 km^2, the cold-core-peak BT colder than 220 K, and the duration over 5 hours. Notably, anvil clouds in this work only refer to the pixels of the BT at 10.8 μm colder than 260 K and the precipitation less than 1 mm/hour.

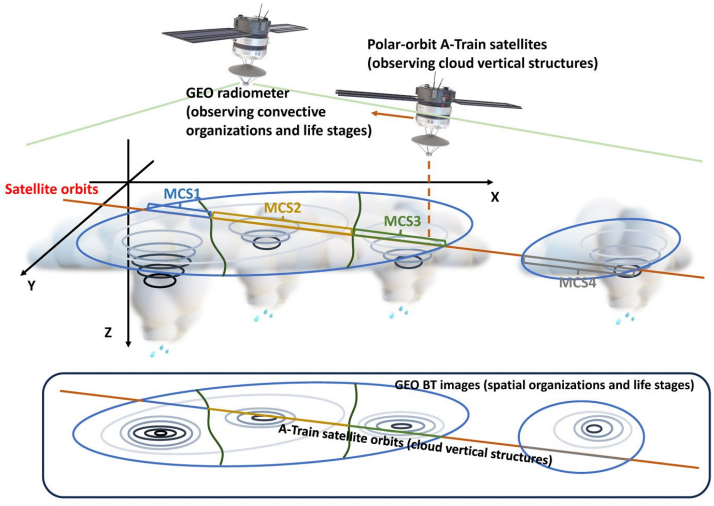

Figure 1. Schematic diagram of the GATM convective cloud data product.

2.2 The GATM convective cloud data product

The schematic diagram of the GATM convective cloud data product is presented in Figure 1. This product is designed to combine the GEO-based MCS tracking and the A-Train satellite-detected cloud vertical profiles. The GEO-based MCS tracking provides the information of convective organizations and life stages, while the A-Train satellites provide the information of cloud vertical structures. The GATM combines the advantage of the GEO radiometer imagers in tracking and the advantage of the A-Train active sensors in detecting cloud vertical structures. Thus, the GATM provides a unique perspective to capture the process-level convective anvil outflow in 4 dimensions of space (x, y and z) and time.

The GEO-based MCS tracking data set was provided in Wang and Yuan (2024) and briefly introduced in Section 2.1. In A-Train Constellation, CALIOP operates at the wavelength of 1024 nm and 532 nm and is sensitive to small particles but easily attenuated for thick clouds. 95-GHz CPR can penetrate thick clouds but usually miss thin cirrus clouds and the upper

https://doi.org/10.5194/egusphere-2025-48
Preprint. Discussion started: 24 January 2025

portion of deep clouds, owing to its low sensitivity to small ice crystals. The CERES instrument measures broadband top-of-atmosphere (TOA) radiances. The Moderate Resolution Imaging Spectroradiometer (MODIS) derives cloud properties based on the CERES cloud algorithm. The capabilities of these instruments were merged in the CALIPSO-CloudSat-CERES-MODIS (CCCM) product (Kato et al., 2010), to provide cloud and radiance measurements. In this product, LW and SW irradiance profiles and cloud profiles are accessible.

The GEO-based MCS tracking and the CCCM are simply collocated by using longitude and latitude, as illustrated in Figure 1. The CCCM profile is matched with the nearest grids of 0.05° resolution. Furthermore, for this CCCM-matched grid, the information of the MCS spatial organizations (such as the distance to the cold core and the cold-core BT) and the temporal evolutions (developing, peaking or decaying, and cold-core-peak BT) are derived from the GEO-based MCS tracking data set to match the CCCM profile.

2.3 Study domain

The study region is selected as the Tropical West Pacific (TWP, 130°W-170°E, 20°S-20°N). Convective activities and anvil clouds are common in this region but the net radiation shows small differences compared with nonconvecting regions. Thus, it is a typical region for investigating the oceanic convection and radiation cancellation. The study time is constrained in June, Jule and August between 2006 and 2011, to avoid the influence of seasonal cycles. For quality control, the tracked life cycles touching the edges or involving missing images are excluded from analyses.

2.4 Statistical methods

The 95% confidence interval for the mean value was computed via the t test: $\bar{x} \pm t_c \frac{s}{\sqrt{N}}$, where $\bar{x}$ is the mean value of all samples; t_c is the critical value for t; and s is the standard deviation of all the samples. N is the number of independent samples, which is determined based on the e-folding length of autocorrelation (Bretherton et al., 1999).

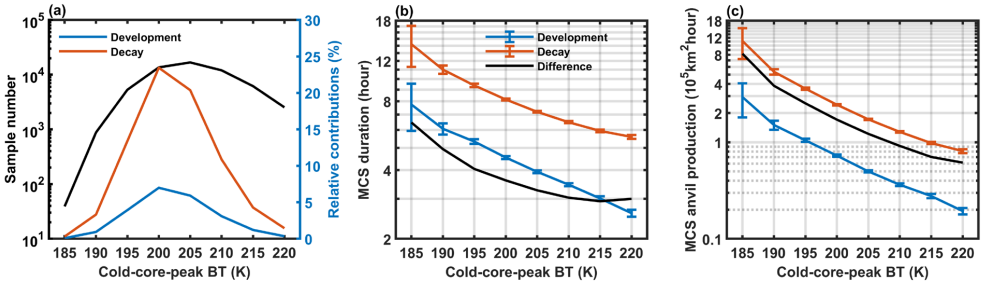

Figure 2. Life cycles of MCSs via adaptive variable-BT tracking. (a) The sample number of the tracked MCS life cycles of different cold-core-peak BT in June-August from 2006 to 2011 over the TWP. The blue and red lines are the relative contribution fractions to total anvil areas for development and decay stages, respectively. The average duration (b) and anvil productivity (c) of different convective strengths. The blue and red represent the quantities of the development and decay stages, respectively. The black line indicates their differences. The error bars indicate the 95% confidence intervals of the means based on the t test.

3 How does the radiation influence the diurnal variation of convective anvil outflow?

In the novel Lagrangian-view convective cloud data product, anvil clouds in CCOs are assigned to MCSs, and the vertical cloud and radiative-heating structures of MCSs are provided. The quantification of MCS anvil production via tracking and the cross section of MCS structures detected by A-Train active sensors are accessible. In this section, the basic features of MCS life cycles are presented in Section 3.1. The diurnal variation of convective anvil outflow and its underlying radiative mechanism are investigated in Section 3.2.

https://doi.org/10.5194/egusphere-2025-48
Preprint. Discussion started: 24 January 2025

3.1 Life cycles of MCSs via adaptive variable-BT segment tracking

The life cycles of MCSs are sorted by the cold-core-peak BT, which represents different convective peaking strengths of MCSs. The colder the cold-core-peak BT is, the stronger the MCS is. The life cycle is separated into two stages: development (before peaking) and decay (peaking and after peaking). Figure 2 shows the basic characteristics of the tracked MCSs over the warm pool of the TWP in June, July and August during 2006-2011.

In Figure 2a, during the observation period over the TWP, the MCSs of the peak BT at 205 K have the highest occurrence frequency, with the sample number of 16744. The MCSs of the peak BT at 185 K have the lowest occurrence frequency, with the sample number of only 39. For different peaking strengths of MCSs, their relative contributions to anvil areas are computed as the sum of the anvil areas produced by the MCSs in each bin of cold-core-peak BT values in development and decay stages, respectively, divided by the total anvil areas produced by all observed MCSs. Overall, the decay stage of MCSs contributes to 77.5% of total anvil areas, whereas the development stage has relatively small anvil contribution fraction of 22.5%.

Figure 2b and Figure 2c show the average duration and anvil production of MCSs in two stages of development and decay, respectively. Here, the anvil production refers to the accumulation of anvil areas for the tracked MCS durations, i.e., the lifetime-accumulated anvil areas. Notably, the Y axes in Figures 2b-c are displayed at the log scale. Thus, the average duration and anvil production conform to loglinear relationships with the cold-core-peak BT. It implies that the average duration and anvil production increase exponentially with colder peak BT values, and thereby the MCSs of colder peak BT values would be much more long-lived and efficient at producing anvil clouds. On average, the tracked duration for the weakest MCSs of the peak BT at 220 K is 8.2 hours, with the development of 2.6 hours and the decay of 5.6 hours. In contrast, the strongest MCSs of the peak BT at 185 K can persist 21.9 hours on average, in which the development takes 7.7 hours and the decay takes 14.2 hours. For the anvil production, anvil clouds produced by the strongest MCSs are approximately14 times those of the weakest MCSs and most of anvil clouds are produced in the MCS decay stage. With MCSs peaking at colder BT values, the difference of duration and anvil production between the development and decay stages (the black lines in Figures 2b-c) also has an exponential increase roughly. It manifests that the decay process of MCSs corresponds to the main process of convective anvil outflow.

Overall, the MCS anvil production has a strong dependence on the convective peaking strength, with a log-linear relationship with the cold-core-peak BT. Thus, it is necessary to distinguish the convective strength for discussing the response of convective anvil outflow to the radiation. In the MCS life cycle, the decay process of MCSs is mainly responsible for the anvil-producing process. For the total anvil cloud budget, the MCSs of the cold-core-peak BT at 200-205 K are the most important, since warmer MCSs are not efficient at producing anvil clouds and colder MCSs are less frequent.

https://doi.org/10.5194/egusphere-2025-48
Preprint. Discussion started: 24 January 2025

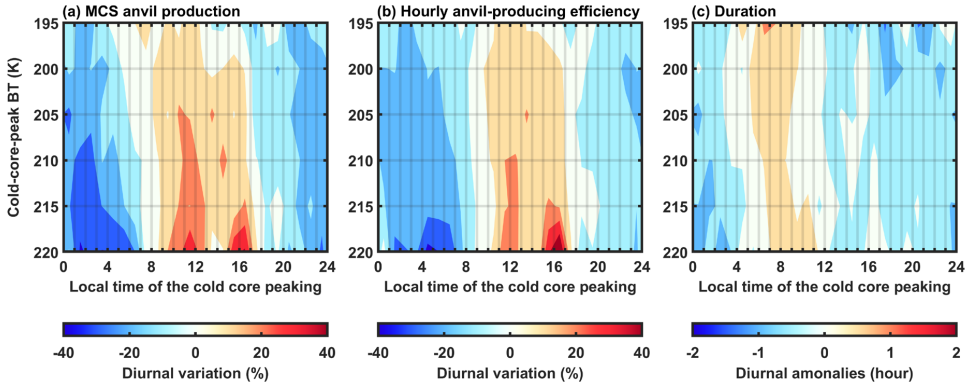

Figure 3. Diurnal variations of the MCS producing the anvil. (a-c) Observed diurnal variations of MCS anvil production, hourly-mean anvil-producing efficiency and duration in the decay stage, respectively.

3.2 Observed diurnal variations of convective anvil outflow and its modulation by radiation

To investigate the variability of MCS anvil production on the diurnal time scale, the MCSs of different peaking strengths are discussed separately. In this way, the convection strength is constrained by the cold-core-peak BT. For the same convection strength, the diurnal variation of the MCSs that peak at different local times is shown in Figure 3.

Here, only the MCSs of the peak BT from 195-220 K and the decay process are considered. The MCSs of the peak BT at 185-190 K account for 4.6% of the anvil contribution and have only 918 samples, which are insufficient to investigate the variations on the diurnal time scale. The MCSs of the peak BT at 195 K have 5310 samples and warmer MCSs are more for investigating their diurnal variations. In addition, the MCS of different local times will experience very distinct radiative heating profiles on the diurnal time scales, which can significantly influence the development and decay stages both. Here, only the decay process of MCSs is discussed, since most anvil clouds are produced from the decay process. As a result, the diurnal difference in the MCS anvil production in Figure 3 can be understood as variations in the MCS decay process accompanied by different radiative heating profiles.

For the same convective peaking strength, the diurnal variation is quantified by the diurnal anomalies at different local times divided by the mean value. In Figure 3a, the MCS anvil production shows a significant diurnal cycle. Overall, daytime-peak MCSs can produce more anvil clouds than nocturnal-peak MCSs in their decay processes. The MCS anvil production can be further decomposed into the hourly anvil-producing efficiency (Figure 3b) and duration (Figure 3c), respectively. Here, the hourly anvil producing efficiency refers to the hourly mean anvil area produced in the MCS decay process. The hourly anvil-producing efficiency experiences a significant diurnal cycle with the amplitude up to approximately 40% of the average value. But the amplitude of the MCS duration anomalies is less than one hour. It manifests that the diurnal variation in the MCS anvil production is mainly explained by the variation in the hourly efficiency of producing anvils but not the duration variation. Similarly, Wall et al. (2020) also reported that the daytime convection can produce more anvil clouds based on wind tracking. They inferred that the diurnal increase in the anvil production results from the prolonged lifetime or larger spread areas of anvil clouds. It is confirmed that the convection of the peaking time between 06:00 and 12:00 LT can persist a longer lifetime as shown in Figure 3c, but the diurnal-cycle amplitude of the MCS duration is relatively small. Higher anvil-producing efficiency (or larger spread areas of anvil clouds) during daytime seems to be the main reason for the diurnal variation in the MCS anvil production.

https://doi.org/10.5194/egusphere-2025-48
Preprint. Discussion started: 24 January 2025

Radiative heating is the fundamental explanation for the diurnal variation of convection. Radiation provides the main impetus for large-scale circulation adjustments on the diurnal time scale to result in the diurnal variation of convection (Ruppert and Hohenegger, 2018). Two mechanisms have been proposed to explain the modulation of the circulation and convective anvil outflow by radiative-heating vertical and horizonal gradients, respectively:

(1) **The lapse-rate mechanism (vertical):** The radiative-heating vertical destabilization of the cloud layer stimulates the in-cloud convection and promotes microphysical recycling, thus to increase the convective anvil outflow (Lilly, 1988; Hartmann et al., 2018).

(2) **The differential radiation mechanism (horizontal):** The horizontal gradient of the radiative heating between anvil clouds and the surrounding clear sky invigorates the upper-level circulation, thus to increase the convective anvil outflow (Gray and Jacobson, 1977; Nicholls, 2015; Wall et al., 2020);

These two mechanisms are both reasonable. But, validating them requires the quantity of convective anvil outflow, which is neither well parameterized in models nor provided in the previous observational cloud data product.

On the basis of the novel GATM convective cloud data product, all relevant measurements of radiance and atmospheric states are provided for the daytime-peak (13:30 LT) and nocturnal-peak (01:30 LT) MCSs, whose diurnal variation is shown in Figure 3. These measurements can be further used to calculate the structure of convective anvil outflow in MCSs according to the thermodynamic energy equation at steady state and continuity function (Thompson et al., 2017):

$$\vec{V} \cdot \nabla_h T - \omega S = Q, \tag{1}$$

$$D = -\frac{\partial \omega}{\partial p} = \frac{\partial}{\partial p}\left(\frac{Q}{S}\right) + \frac{\partial}{\partial p}\left(\frac{-\vec{V}\cdot\nabla_h T}{S}\right). \tag{2}$$

$\vec{V} \cdot \nabla_h T$ is the horizontal temperature advection, ω is the vertical velocity in pressure coordinates, S is the stability ($-\frac{T}{\theta}\frac{\partial \theta}{\partial p}$), Q is the diabatic heating, and D is the divergence. In tropics, with weak horizontal gradient of temperature, the divergence is largely caused by the radiative heating and can be simplified as $\frac{\partial}{\partial p}\left(\frac{Q}{S}\right)$. As a result, the divergence directly caused by the radiative heating in the MCSs corresponds to the lapse-rate mechanism, whereas the circulation invigorated by the difference of radiative heating between MCSs and the surrounding clear-sky environment corresponds to the differential radiation mechanism. The radiative impacts of these two mechanisms on the diurnal variation of convective anvil outflow are discussed separately as follows.

For the lapse-rate mechanism, the heating rate (Q, Figures 4a-d), heating destabilization ($\frac{\partial Q}{\partial p}$, Figures 4e-h) and radiation-driven divergence ($\frac{\partial}{\partial p}\left(\frac{Q}{S}\right)$, Figures 4i-l) caused by LW, SW and net radiances are investigated for the MCSs of the cold-core-peak at 13:30 LT (left panels in Figure 4) and 01:30 LT (right panels in Figure 4), respectively. The MCS cloud structure is represented by the cloud fraction (the black contours in Figure 4), which is defined as the ratio of cloud occurrence to the number of all samples. The region with high values of the cloud fraction can be understood as the main cloud domain. For either 13:30 or 01:30 LT, clouds have well organized structures in MCSs. A convective pillar that is shaped by cloud-fraction contours exists within 50 km around the MCS cold core. Away from the convective pillar, clouds concentrate on the layer between approximately 12-14 km, which well shapes the convective anvil outflow.

At 13:30 LT, LW cooling is nearly completely offset by SW heating, and the MCS is experiencing strong net radiative heating, as shown in Figure 4a-c. In the vertical direction, the net heating of the MCS top has a rapid decline from approximately 13 to 16 km (Figure 4c). The vertical decline of the heating can lead to the radiative destabilization (Figure 4g) and thereby strong convective outflow (Figure 4k) at the MCS top. Overall, the convective outflow at 13:30 LT should be largely attributed to the divergence caused by the SW heating destabilization (Figure 4f and 4g), whereas the LW heating

https://doi.org/10.5194/egusphere-2025-48
Preprint. Discussion started: 24 January 2025

stabilizes the MCS top (Figure 4e) and contributes to little or even negative outflow (Figure 4i).

At 01:30 LT, only LW cooling exists (Figure 4d). And the decline of the LW cooling stabilizes the MCS top (Figure 4h) to inhibit the divergence (Figure 4l). In summary, daytime SW heating destabilizes the MCS top to promote anvil outflow, whereas nighttime LW cooling stabilizes the MCS top to reduce anvil outflow. This day-night difference of radiative destabilization (the lapse-rate mechanism) well explains the diurnal variation of convective outflow presented in Figure 3. It is also interesting to notice that the nighttime MCSs accompanied with weak divergence seem to have thicker anvil clouds in comparison with the daytime MCS structure shaped by cloud-fraction contours, although the anvil thickness is not the focus of this work.

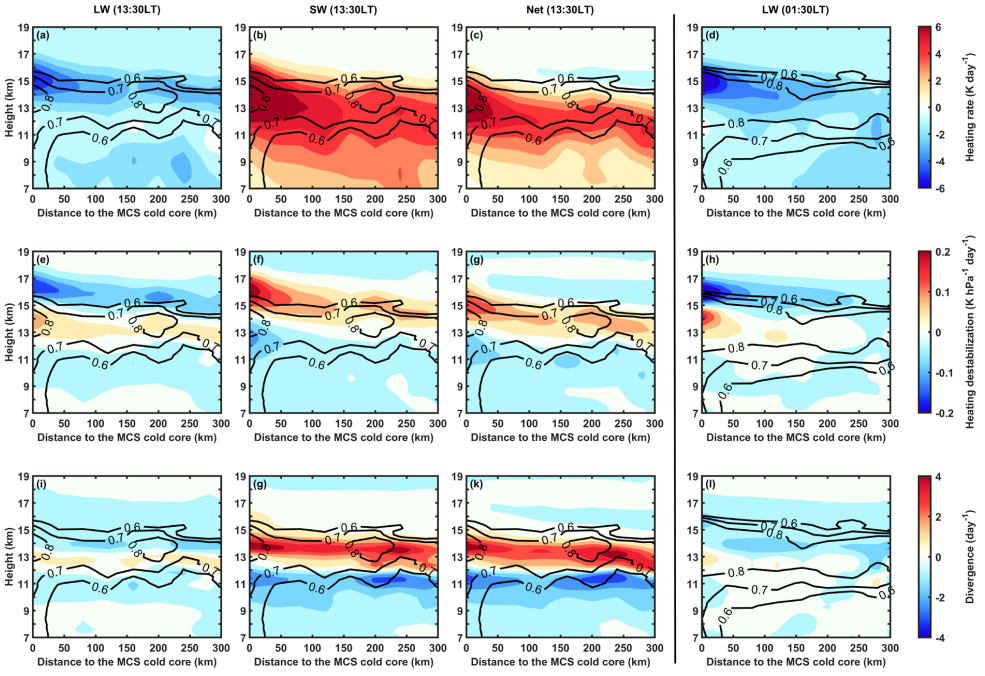

Figure 4. Radiative heating rate, heating destabilization and divergence caused by LW, SW and net radiances for MCSs at 13:30 and 01:30 LT, respectively. (a-c) The LW, SW and net heating rate at 13:30 LT. (d) The LW heating rate at 01:30 LT. (e-h) and (i-l) similar to (a-d) but for heating destabilization and divergence. The black contours represent cloud fraction.

For the differential radiation mechanism, the circulation between the MCS and its surrounding clear-sky environments results from the balance between the MCS divergence and the clear-sky convergence. Thus, the circulation can be enhanced by stronger MCS divergence or stronger clear-sky convergence (or vice versa). This provides a perspective that the clear-sky radiative cooling can constrain the convective development through circulation (Hartmann and Larson, 2002). Gray and Jacobson (1977) and Nicholls (2015) argued that the enhancement of the radiative cooling outside the cloud system can result in stronger clear-sky convergence to promote the circulation, and ultimately leading to the development of convection. From the perspective of the circulation between the MCS and its surrounding clear sky, the circulation can be split into two parts: cloudy-sky divergence and clear-sky convergence. The divergence at the MCS top is enhanced by SW radiative heating during the daytime (as discussed above and shown in Figure 4), which can also be understood as the enhancement of a half circulation caused by the SW heating. Another half circulation depends on the convergence driven by the clear-sky radiative cooling and is further investigated in Figure 5. At 13:30 LT, LW radiative cooling is partially offset by the SW radiative heating (Figure 5a), and the stabilization (Figure 5c) and convergence (Figure 5e) caused by the LW cooling is weakened by the SW heating. At 01:30 LT, only LW cooling is available and the convergence driven by the net radiative

https://doi.org/10.5194/egusphere-2025-48
Preprint. Discussion started: 24 January 2025

cooling (Figure 5f) is stronger than that at 13:30 LT. Overall, stronger net cooling at the night leads to stronger clear-sky convergence, which is more favorable for the development of convection from the perspective of the circulation. However, it cannot explain the diurnal variation of the convective anvil outflow, which peaks at the daytime. Overall, from the perspective of the circulation, the diurnal variation of convective anvil outflow should be attributed to the top-heavy circulation enhanced by the SW radiative heating to MCSs during the daytime, but is not determined by the diurnal variation in the surrounding clear-sky radiative cooling.

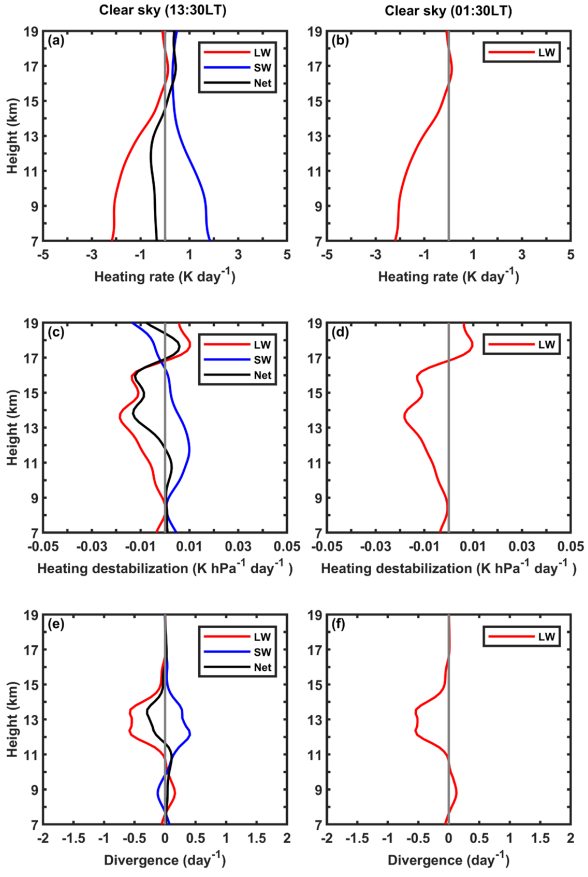

Figure 5. Radiative heating rate, heating destabilization and divergence caused by LW, SW and net radiances for the clear sky at 13:30 and 01:30 LT, respectively. (a) The LW, SW and net heating rate at 13:30 LT. (b) The LW heating rate at 01:30 LT. (c-d) and (e-f) similar to (a-b) but for heating destabilization and divergence. The red, blue and black lines represent quantities caused by LW, SW and net radiances, respectively.

4 How does the diurnal variation of convective anvil outflow influence the radiative cancellation?

The non-precipitating anvil outflow of MCSs is an important component of the cloud water budget and imposes a strong forcing on the Earth radiative energy budget (Zhao et al., 2016). But the water and radiative budgets have a non-linear relationship, which means the radiative energy budget cannot be simply inferred from the variation in the anvil amount. A key parameter that determines the non-linear cloud-radiation relationship is the local time of the convection producing the anvil. Different local times correspond to various insolation strengths and surface outgoing longwave radiation. Thus, at different local times, clouds of the same radiative properties (i.e., albedo and longwave radiative emission) can have completely different radiative effects. In this section, the sensitivity of the radiative energy budget to the diurnal variation in the cloud water budget

https://doi.org/10.5194/egusphere-2025-48
Preprint. Discussion started: 24 January 2025

is investigated.

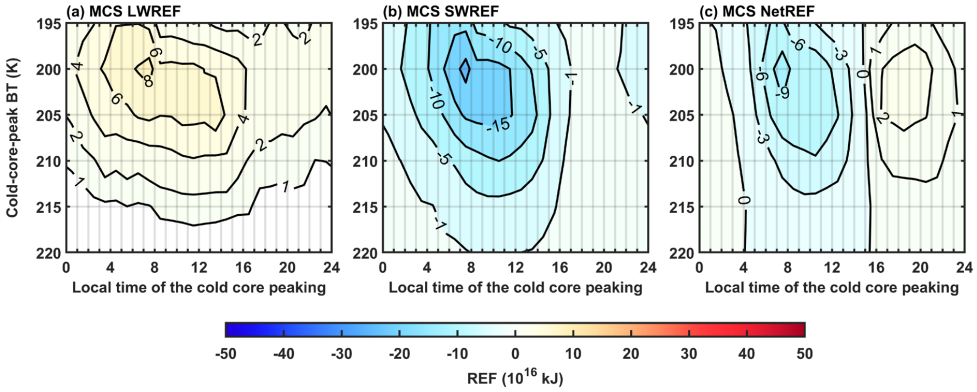

Figure 6. Radiative cancellation on the diurnal time scale. (a-c) The LWREF, SWREF and NetREF induced by the MCSs of different peaking strengths and times.

In Figure 6, the TOA radiative budget contributed by MCSs of different convective strengths and peaking times are shown. Only the decay process is considered. The radiative energy forcing (REF) represents the changes of the TOA radiative energy budget forced by the MCS anvil production. The positive sign implies warming effects and the negative sign implies cooling effects on the Earth.

The cancellation ratio between LW (Figure 6a) and SW (Figure 6b) REFs is not constant on the diurnal timescale, but has a strong dependence on the peaking local time of MCSs. As shown in Figure 6c, for the anvil production by MCSs of the peak between 04:00-15:00 local time, their SW REFs are partially cancelled by the LW REFs, which leads to a net cooling effect. On the other hand, for the MCSs of other peaking local times, their SW REFs are completely cancelled by the LW REFs, with a net warming effect. Ultimately, a secondary radiation cancellation between the net cooling and warming occurs on the diurnal timescale. 27% of the net cooling are further cancelled by the net warming on the diurnal time scale.

This cancellation is not surprising, but it is interesting to wonder what determines this secondary net radiation cancellation ratio. There is no doubt that the cloud-top height (Kiehl, 1994) and anvil area coverage (Hartmann and Berry, 2017) are two important determinants to modulate this cancellation ratio. If all radiative properties of anvil clouds have no changes but only the diurnal cycle of the MCS anvil production of current climatology has a positive phase shift, the anvil cloud budget would be re-disturbed on the diurnal time scale, with relatively more daytime anvil clouds and less nighttime anvil clouds. And thus, their SW REFs do not just have a phase shift but the diurnal-cycle amplitude can be further amplified to reduce the secondary net radiation cancellation ratio and increase net cooling effects. This simple example suggests that the secondary net radiation cancellation ratio is sensitive to diurnal variation of MCS anvil production. For distinct climatology of the diurnal variation of MCS anvil production, the secondary net radiation cancellation ratio varies.

https://doi.org/10.5194/egusphere-2025-48
Preprint. Discussion started: 24 January 2025

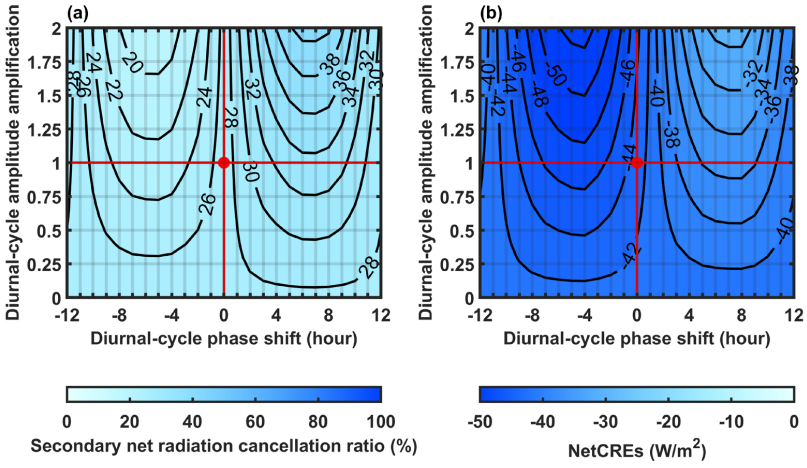

Figure 7. Sensitivity of the net radiative cancellation to diurnal variations of the MCS producing the anvil. (a-b) The sensitivity of the secondary net radiation cancellation ratio and net CREs, respectively, to distinct climatology of diurnal variation of MCS anvil production. The red dot represents the current climatology of the diurnal cycle.

The sensitivity of the secondary net radiation cancellation to the diurnal variation of convective anvil outflow is evaluated in Figure 7. A linear model of the net REF (NetREF) to the MCS anvil production is constructed as:

$$NetREF(\mathrm{BT},\ LT) = F(\mathrm{BT},\ LT)[\alpha A(\mathrm{BT},\ LT) + \beta]. \quad (3)$$

F and A represent the occurrence frequency and anvil production, respectively. NetREF, F and A all are functions of the local time (LT) and the cold-core-peak BT. α and β are the linear regression coefficient and intercept, respectively. For example, the quantity of $\alpha A_0(BT_0,\ LT_0) + \beta$ in Eq. 3 can be understood as the prediction of the NetREF caused by one MCS of the strength of BT_0 and the anvil production of A_0 at the LT_0 local time. Here, we only focus on the diurnal variation of A.

By multiplying the predicted NetREF of $A(\mathrm{BT},\ LT)$ by the MCS occurrence frequency (F) in Eq. 3, the final NetREF induced by all anvil production of the MCSs of different strengths and peaking local times can be computed. Notably, A is the function of BT (convective strength) and LT (peaking time). And the diurnal cycle of A is tunable and can be further expressed as:

$$A(BT, LT) = \overline{A_{obs}(BT)} + \lambda[A_{obs}(BT, LT - \delta) - \overline{A_{obs}(BT)}]. \quad (4)$$

The subscript obs represents the value derived from observations. The bar over the letter head represents the mean value. λ refers to the diurnal-cycle amplitude amplification ratio. δ refers to the diurnal-cycle phase shift. For $\lambda = 1$ and $\delta = 0$, A has the diurnal cycle that is consistent with the observation presented in Figure 3a. By altering λ and δ, the observed diurnal-cycle amplitudes and phases of A in Figure 3a can be tuned. In this way, A of different diurnal cycles in Eq. (4) can be further input to the linear model of Eq. 3 to evaluate the sensitivity of the secondary net radiation cancellation ratio to the diurnal cycle of A, as shown in Figure 7. Here, the secondary net radiation cancellation ratio refers to the cancellation ratio between the net cooling and warming that occurs on the diurnal time scale (27% for the current climatology of diurnal cycles). The net CRE (NetCRE) is defined as the $NetREF/(F \times A)$, which can be understood as the sensitivity of the net radiative budget to the anvil-amount variation under different climatology of diurnal cycles.

Figure 7 shows that the net radiation cancellation and NetCREs vary with the changes in the climatology of diurnal cycle of convective anvil outflow. If current climatology of the A diurnal cycle has positive phase shifts or weaker amplitude, more anvils would be distributed at the night and the secondary cancellation would be enhanced to make the Earth warmer

https://doi.org/10.5194/egusphere-2025-48
Preprint. Discussion started: 24 January 2025

than the current state (or vice versa). If the amplitude is constant, approximately 10% for the secondary cancellation and 11 W m^{-2} K^{-1} for CREs can be simply modulated by the diurnal phase of convective anvil outflow. In contrast, the assessed high-cloud altitude and anvil coverage feedback strengths in climate models are only 0.2 and -0.2 W m^{-2} K^{-1}, respectively (Sherwood et al., 2020). Although The diurnal-cycle feedback and its relevant mechanism is still missing in current climate studies, cloud-resolving models and observations both suggested that the diurnal cycle of clouds can respond to the climate change with a positive phase shift with surface temperature rising (Yin and Porporato, 2019; Gasparini et al., 2021; Wang et al., 2022). The high sensitivity of the radiative cancellation to the diurnal variation of convective anvil outflow (Figure 7) suggests that this diurnal-cycle climate feedback could be an important but missing component for the climate sensitivity.

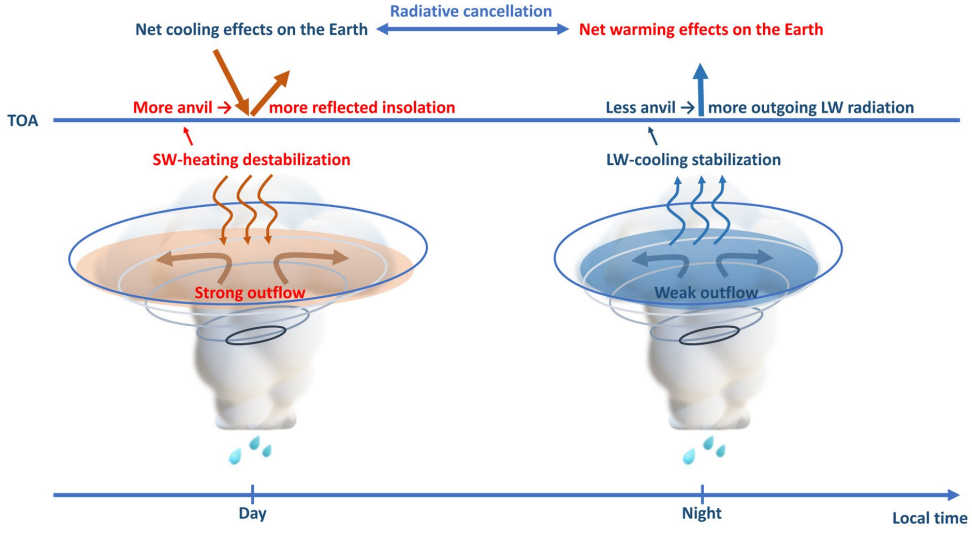

Figure 8. Illustrations of the anvil-radiation diurnal interaction processes.

5 Conclusions

Tropical convection usually has complex convective organizations. Many convections in different life stages are clustered in complex organizations and their produced anvil clouds are merged. As a result, the process of convective anvil outflow has been poorly distinguished in observations for complex convective organizations.

The observed process of convection producing anvil clouds is the key reference for understanding the convective water budget and developing model convection parameterization. Nevertheless, conventional Euler-view observational product provides limited reference for this process. For example, the GEO-based cloud grid data product (e.g., ISCCP and CERES project) provides little information of the sub-grid convective organizations and the links between convection and anvil clouds. Although the cloud data product based on the sensors of A-Train Constellation (i.e., CCCM) provides cloud and radiance vertical structures, the full picture of horizonal convective organizations and the life stage of convection are not accessible. In this work, to provide observational reference for convective anvil outflow in complex organizations, the advantages of GEOs and A-Train Constellation are combined with two steps:

(1) Via GEO observations and the adaptive variable-BT segment tracking algorithm, the complex convective organizations of many connected MCSs are decomposed into single MCSs for tracking separately. In this way, anvil clouds are explicitly associated with unique MCSs, which provides the foundation to investigate the process of convective anvil outflow in complex organizations.

https://doi.org/10.5194/egusphere-2025-48
Preprint. Discussion started: 24 January 2025

(2) Via matching the CCCM data product, the corresponding cloud and radiance vertical structures for these tracked MCSs are retrieved.

In this way, the advantage of the GEO for observing cloud organization and tracking and the advantage of A-Train Constellation for detecting cloud and radiance vertical structures are merged in GATM convective cloud data product. The aim of the GATM is to resolve cloud and radiance structures of convective anvil outflow in complex organizations under a Lagrangian view.

Based on the GATM convective cloud product, the processes of the interaction between radiation and convective anvil outflow are summarized in Figure 8 and described as follows:

(1) **The diurnal variation of convective anvil outflow is primarily driven by the SW radiative heating to clouds.** The results show that daytime SW radiative heating destabilizes the MCS top to enhance the convective anvil outflow. Nighttime LW radiative cooling stabilizes the MCS top to reduce the convective anvil outflow. According to the anvil-radiation mechanisms proposed in previous studies, this is well consistent with the lapse-rate mechanism (the vertical heating structure determines the anvil outflow). For the differential radiation mechanism (the horizontal heating difference determines the anvil outflow), it gives a circulation perspective between convective region and its surrounding clear sky to understand the anvil outflow, and suggests that larger clear-sky convergence can promote stronger convection. However, the results show that there is little diurnal variation in the clear-sky radiative-driven convergence. Nevertheless, it is reasonable that daytime SW radiative heating promotes divergence to strengthen the circulation. As a result, from the perspective of either the lapse-rate mechanism and the differential radiation mechanism, SW radiative heating to clouds determines the diurnal variation of convective anvil outflow.

(2) **The radiative budget is modulated by the diurnal variation of convective anvil outflow.** Strong daytime anvil outflow and weak nighttime anvil outflow make the anvil be more distributed at the daytime to reflect more insolation but less distributed at the nighttime to trap less outgoing LW radiation. On average, a secondary radiation cancellation between the net cooling and the net warming occurs on the diurnal time scale, with the cancellation ratio of 27%. This cancellation ratio is sensitive to the diurnal variation of convective outflow but has been rarely studied. According to a simple linear model, the result suggests that approximately 10% for the secondary radiative cancellation and 11 W m^{-2} for CREs can be modulated by the diurnal variation of convective anvil outflow.

This work explains the interaction processes between radiation and convective anvil outflow on the diurnal time scale. The radiative budget is sensitive to the diurnal variation of the anvil outflow. Under different climatology of the diurnal variation of the anvil outflow, the mean CRE can have the variation up to 11 W m^{-2}. However, the assessed high-cloud altitude and anvil coverage feedback strengths in climate models are only 0.2 and -0.2 W m^{-2} K^{-1}, respectively (Sherwood et al., 2020). It implies that the response of the diurnal variation of the anvil outflow to the climate could be a large component in cloud-climate feedback, but has not been well studied until now. This work suggests that the SW radiative heating to clouds can explain the diurnal variation of anvil outflow, but it does not guarantee that the diurnal variation of convective anvil outflow is invariant as the climate warms. There is need to investigate the sensitivity of the diurnal variation to the environmental changes in the future work to advance understandings on the cloud-radiation-climate feedback process.

Acknowledgment

This work was supported by the NSFC-41875004 and the National Key R&D Program of China (2016YFC0202000). This work was supported by the Jiangsu Collaborative Innovation Center for Climate Change.

Author contribution

ZW prepared the original manuscript.

https://doi.org/10.5194/egusphere-2025-48
Preprint. Discussion started: 24 January 2025

Data and code availability

All data used in this study are available online. The GEO images are obtained from the National Aeronautics and Space Administration (NASA) Langley Research Center Atmospheric Science Data Center (https://doi.org/10.5067/MTS01/CERES, NASA/LARC/SD/ASDC, 2017). The GPM is obtained from the Goddard Earth Sciences Data and Information Services Center (GES DISC) at https://doi.org/10.5067/GPM/IMERG/3BHH/07 (Huffman et al., 2023). The CCCM data product are obtained from the National Aeronautics and Space Administration (NASA) Langley Research Center Atmospheric Science Data Center (https://search.earthdata.nasa.gov/). The code is available upon request.

Competing interests

The author declares that he has no conflict of interest.

Reference

Atlas, R. L., Bretherton, C. S., Sokol, A. B., Blossey, P. N., and Khairoutdinov, M. F.: Tropical Cirrus Are Highly Sensitive to Ice Microphysics Within a Nudged Global Storm-Resolving Model, Geophysical Research Letters, 51, e2023GL105868, 10.1029/2023gl105868, 2024.

Bretherton, C. S.: Insights into low-latitude cloud feedbacks from high-resolution models, Philos Trans A Math Phys Eng Sci, 373, 20140415, 10.1098/rsta.2014.0415, 2015.

Bretherton, C. S., Widmann, M., Dymnikov, V. P., Wallace, J. M., and Bladé, I.: The Effective Number of Spatial Degrees of Freedom of a Time-Varying Field, Journal of Climate, 12, 1990-2009, 10.1175/1520-0442(1999)012<1990:Tenosd>2.0.Co;2, 1999.

Chen, G., Wang, W. C., Bao, Q., and Li, J.: Evaluation of Simulated Cloud Diurnal Variation in CMIP6 Climate Models, Journal of Geophysical Research: Atmospheres, 127, 10.1029/2021jd036422, 2022.

Clement, A. C. and Soden, B.: The Sensitivity of the Tropical-Mean Radiation Budget, Journal of Climate, 18, 3189-3203, 10.1175/jcli3456.1, 2005.

Doelling, D. R., Sun, M., Nguyen, L. T., Nordeen, M. L., Haney, C. O., Keyes, D. F., and Mlynczak, P. E.: Advances in Geostationary-Derived Longwave Fluxes for the CERES Synoptic (SYN1deg) Product, Journal of Atmospheric and Oceanic Technology, 33, 503-521, 10.1175/jtech-d-15-0147.1, 2016.

Gasparini, B., Rasch, P. J., Hartmann, D. L., Wall, C. J., and Dütsch, M.: A Lagrangian Perspective on Tropical Anvil Cloud Lifecycle in Present and Future Climate, Journal of Geophysical Research: Atmospheres, 126, 10.1029/2020jd033487, 2021.

Gettelman, A. and Sherwood, S. C.: Processes Responsible for Cloud Feedback, Current Climate Change Reports, 2, 179-189, 10.1007/s40641-016-0052-8, 2016.

Gray, W. M. and Jacobson, R. W.: Diurnal Variation of Deep Cumulus Convection, Monthly Weather Review, 105, 1171-1188, 10.1175/1520-0493(1977)105<1171:Dvodcc>2.0.Co;2, 1977.

Hartmann, D. L.: Tropical anvil clouds and climate sensitivity, Proceedings of the National Academy of Sciences, 113, 8897-8899, 10.1073/pnas.1610455113, 2016.

Hartmann, D. L. and Berry, S. E.: The balanced radiative effect of tropical anvil clouds, J Geophys Res-Atmos, 122, 5003-5020, 10.1002/2017jd026460, 2017.

Hartmann, D. L. and Larson, K.: An important constraint on tropical cloud - climate feedback, Geophysical Research Letters, 29, 10.1029/2002gl015835, 2002.

Hartmann, D. L., Gasparini, B., Berry, S. E., and Blossey, P. N.: The Life Cycle and Net Radiative Effect of Tropical Anvil Clouds, Journal of Advances in Modeling Earth Systems, 10, 3012-3029, 10.1029/2018ms001484, 2018.

Huffman, G. J., E.F. Stocker, D.T. Bolvin, E.J. Nelkin, Jackson Tan: GPM IMERG Final Precipitation L3 Half Hourly 0.1 degree x 0.1 degree V07, Goddard Earth Sciences Data and Information Services Center (GES DISC), 10.5067/GPM/IMERG/3B-HH/07, 2023.

Kato, S., Sun-Mack, S., Miller, W. F., Rose, F. G., Chen, Y., Minnis, P., and Wielicki, B. A.: Relationships among cloud occurrence

https://doi.org/10.5194/egusphere-2025-48
Preprint. Discussion started: 24 January 2025

frequency, overlap, and effective thickness derived from CALIPSO and CloudSat merged cloud vertical profiles, Journal of Geophysical Research: Atmospheres, 115, 10.1029/2009jd012277, 2010.

Kiehl, J. T.: On the Observed Near Cancellation between Longwave and Shortwave Cloud Forcing in Tropical Regions, Journal of Climate, 7, 559-565, 10.1175/1520-0442(1994)007<0559:Otoncb>2.0.Co;2, 1994.

Lilly, D. K.: Cirrus Outflow Dynamics, Journal of the Atmospheric Sciences, 45, 1594-1605, 10.1175/1520-0469(1988)045<1594:Cod>2.0.Co;2, 1988.

Matsui, T., Zeng, X., Tao, W.-K., Masunaga, H., Olson, W. S., and Lang, S.: Evaluation of Long-Term Cloud-Resolving Model Simulations Using Satellite Radiance Observations and Multifrequency Satellite Simulators, Journal of Atmospheric and Oceanic Technology, 26, 1261-1274, 10.1175/2008jtecha1168.1, 2009.

Minnis, P., Sun-Mack, S., Young, D. F., Heck, P. W., Garber, D. P., Chen, Y., Spangenberg, D. A., Arduini, R. F., Trepte, Q. Z., Smith, W. L., Ayers, J. K., Gibson, S. C., Miller, W. F., Hong, G., Chakrapani, V., Takano, Y., Liou, K.-N., Xie, Y., and Yang, P.: CERES Edition-2 Cloud Property Retrievals Using TRMM VIRS and Terra and Aqua MODIS Data—Part I: Algorithms, IEEE Transactions on Geoscience and Remote Sensing, 49, 4374-4400, 10.1109/tgrs.2011.2144601, 2011.

Nicholls, M. E.: An investigation of how radiation may cause accelerated rates of tropical cyclogenesis and diurnal cycles of convective activity, Atmos. Chem. Phys., 15, 9003-9029, 10.5194/acp-15-9003-2015, 2015.

Powell, S. W., Houze, R. A., Kumar, A., and McFarlane, S. A.: Comparison of Simulated and Observed Continental Tropical Anvil Clouds and Their Radiative Heating Profiles, Journal of the Atmospheric Sciences, 69, 2662-2681, 10.1175/jas-d-11-0251.1, 2012.

Rossow, W. B. and Schiffer, R. A.: ISCCP Cloud Data Products, Bulletin of the American Meteorological Society, 72, 2-20, 10.1175/1520-0477(1991)072<0002:Icdp>2.0.Co;2, 1991.

Ruppert, J. H. and Hohenegger, C.: Diurnal Circulation Adjustment and Organized Deep Convection, Journal of Climate, 31, 4899-4916, 10.1175/jcli-d-17-0693.1, 2018.

Sherwood, S. C., Webb, M. J., Annan, J. D., Armour, K. C., Forster, P. M., Hargreaves, J. C., Hegerl, G., Klein, S. A., Marvel, K. D., Rohling, E. J., Watanabe, M., Andrews, T., Braconnot, P., Bretherton, C. S., Foster, G. L., Hausfather, Z., von der Heydt, A. S., Knutti, R., Mauritsen, T., Norris, J. R., Proistosescu, C., Rugenstein, M., Schmidt, G. A., Tokarska, K. B., and Zelinka, M. D.: An Assessment of Earth's Climate Sensitivity Using Multiple Lines of Evidence, Rev Geophys, 58, e2019RG000678, 10.1029/2019RG000678, 2020.

Stephens, G. L., Vane, D. G., Boain, R. J., Mace, G. G., Sassen, K., Wang, Z., Illingworth, A. J., O'Connor, E. J., Rossow, W. B., Durden, S. L., Miller, S. D., Austin, R. T., Benedetti, A., and Mitrescu, C.: The Cloudsat Mission and the a-Train, Bulletin of the American Meteorological Society, 83, 1771-1790, 10.1175/bams-83-12-1771, 2002.

Suzuki, K., Golaz, J. C., and Stephens, G. L.: Evaluating cloud tuning in a climate model with satellite observations, Geophysical Research Letters, 40, 4464-4468, 10.1002/grl.50874, 2013.

Thompson, D. W. J., Bony, S., and Li, Y.: Thermodynamic constraint on the depth of the global tropospheric circulation, Proc Natl Acad Sci U S A, 114, 8181-8186, 10.1073/pnas.1620493114, 2017.

Wall, C. J., Norris, J. R., Gasparini, B., Smith, W. L., Thieman, M. M., and Sourdeval, O.: Observational Evidence that Radiative Heating Modifies the Life Cycle of Tropical Anvil Clouds, Journal of Climate, 33, 8621-8640, 10.1175/jcli-d-20-0204.1, 2020.

Wang, Z. and Yuan, J.: Observing convective activities in complex convective organizations and their contributions to precipitation and anvil cloud amounts, Atmos. Chem. Phys., 24, 13811-13831, 10.5194/acp-24-13811-2024, 2024.

Wang, Z., Ge, J., Yan, J., Li, W., Yang, X., Wang, M., and Hu, X.: Interannual shift of tropical high cloud diurnal cycle under global warming, Climate Dynamics, 59, 3391-3400, 10.1007/s00382-022-06273-6, 2022.

Yin, J. and Porporato, A.: Diurnal cloud cycle biases in climate models, Nature Communications, 8, 10.1038/s41467-017-02369-4, 2017.

Yin, J. and Porporato, A.: Radiative effects of daily cycle of cloud frequency in past and future climates, Climate Dynamics, 54, 1625-1637, 10.1007/s00382-019-05077-5, 2019.

Yuan, J. and Houze, R. A.: Global Variability of Mesoscale Convective System Anvil Structure from A-Train Satellite Data, Journal

https://doi.org/10.5194/egusphere-2025-48
Preprint. Discussion started: 24 January 2025

of Climate, 23, 5864-5888, 10.1175/2010jcli3671.1, 2010.

Yuan, J. and Houze, R. A.: Deep Convective Systems Observed by A-Train in the Tropical Indo-Pacific Region Affected by the MJO, Journal of the Atmospheric Sciences, 70, 465-486, 10.1175/jas-d-12-057.1, 2013.

Yuan, J., Houze, R. A., and Heymsfield, A. J.: Vertical Structures of Anvil Clouds of Tropical Mesoscale Convective Systems Observed by CloudSat, Journal of the Atmospheric Sciences, 68, 1653-1674, 10.1175/2011jas3687.1, 2011.

Zelinka, M. D. and Hartmann, D. L.: Why is longwave cloud feedback positive?, Journal of Geophysical Research, 115, 10.1029/2010jd013817, 2010.

Zeng, X., Tao, W.-K., Powell, S. W., Houze, R. A., Ciesielski, P., Guy, N., Pierce, H., and Matsui, T.: A Comparison of the Water Budgets between Clouds from AMMA and TWP-ICE, Journal of the Atmospheric Sciences, 70, 487-503, 10.1175/jas-d-12-050.1, 2013.

Zhao, M.: An Investigation of the Connections among Convection, Clouds, and Climate Sensitivity in a Global Climate Model, Journal of Climate, 27, 1845-1862, 10.1175/jcli-d-13-00145.1, 2014.

Zhao, M., Golaz, J. C., Held, I. M., Ramaswamy, V., Lin, S. J., Ming, Y., Ginoux, P., Wyman, B., Donner, L. J., Paynter, D., and Guo, H.: Uncertainty in Model Climate Sensitivity Traced to Representations of Cumulus Precipitation Microphysics, Journal of Climate, 29, 543-560, 10.1175/jcli-d-15-0191.1, 2016.

Zhao, Y., Li, J., Zhang, L., Deng, C., Li, Y., Jian, B., and Huang, J.: Diurnal cycles of cloud cover and its vertical distribution over the Tibetan Plateau revealed by satellite observations, reanalysis datasets, and CMIP6 outputs, Atmospheric Chemistry and Physics, 23, 743-769, 10.5194/acp-23-743-2023, 2023.